

# THE ROLE OF NUCLEON RESONANCES IN $\eta'$ PRODUCTION PROCESSES\*

K. NAKAYAMA

Department of Physics and Astronomy, University of Georgia  
Athens, GA 30602, USA  
and

Institut für Kernphysik and Center for Hadron Physics, Forschungszentrum-Jülich  
52425 Jülich, Germany

(Received January 7, 2014)

Based on an effective Lagrangian approach, we performed a combined analysis of the free and quasi-free  $\gamma N \rightarrow \eta' N$ ,  $NN \rightarrow NN\eta'$ , and  $\pi N \rightarrow \eta' N$  reactions. Considering spin-1/2 and -3/2 resonances, we found that a set of above-threshold resonances  $\{S_{11}, P_{11}, P_{13}\}$ , with fitted mass values of about  $M_R = 1925, 2130$ , and  $2050$  MeV, respectively, and the four-star sub-threshold  $P_{13}(1720)$  resonance reproduce best all existing data for the  $\eta'$  production processes from threshold to  $\sqrt{s} \sim 2.35$  GeV. All three above threshold resonances found in the present analysis are essential and indispensable for the good quality of the present fits. A very small  $\eta' N$  scattering length of  $a_{\eta' N} \sim (0.017 + i0.005)$  fm is obtained.

DOI:10.5506/APhysPolB.45.721

PACS numbers: 25.20.Lj, 13.60.Le, 13.75.-n, 14.20.Gk

## 1. Introduction

A wealth of interesting physics can be obtained from studying the production processes involving the  $\eta'$  meson, one of the primary interests being here that such production processes may help one to extract information on nucleon resonances that cannot be obtained from pion reactions. In fact, current knowledge of most of the nucleon resonances is mainly due to the study of  $\pi N$  scattering and/or pion photoproduction off the nucleon. Since the  $\eta'$  meson is much heavier than the pion,  $\eta'$ -meson production processes near threshold, therefore, are well suited for investigating high-mass resonances in low partial-wave states. Furthermore, reaction processes such as  $\eta'$  photoproduction provide opportunities to study, in particular, those resonances

---

\* Presented at the II International Symposium on Mesic Nuclei, Kraków, Poland, September 22–25, 2013.

that couple only weakly to pions. This may help in providing a better understanding of the so-called “missing resonances” predicted by quark models, but not found in more traditional pion-production reactions [1].

Recently, there has also been a particular interest in learning about the  $\eta'N$  interaction in connection with a possibility of formation of the so-called  $\eta'$ -mesic nucleus which is a bound state of  $\eta'$  meson in a nucleus. In fact, there are currently some efforts to search for  $\eta'$ -mesic nuclei [2]. Obviously, the strength of the  $\eta'N$  interaction (including its sign) plays a crucial role in whether or not such a bound state can exist. This is a very important issue for, unlike the  $\eta N$  interaction which is relatively strong with an averaged value of the scattering length of  $a_{\eta N} \sim 0.59 + i0.26$  fm [3], the  $\eta'N$  interaction is expected to be relatively weak. Unfortunately, the information on the  $\eta'N$  interaction are extremely scarce. A recent estimate by Oset and Ramos [4], base on a coupled channel unitized Chiral Perturbation Theory, yields a value of the  $\eta'N$  scattering length in the range of  $a_{\eta'N} = \pm(0.073 - 0.149) + i(0.019 - 0.021)$  fm. On the other hand, based on a purely phenomenological approach, Moskal *et al.* [5] have extracted the  $\eta'N$  scattering length of  $|a_{\eta'N}| \approx 0.1$  fm from the near threshold  $pp$  collision data.

In this work, we perform a combined analysis of the reaction channels  $\gamma N \rightarrow \eta'N$ ,  $NN \rightarrow NN\eta'$ , and  $\pi N \rightarrow \eta'N$  with the particular attention to extracting information on nucleon resonances as well as on the  $\eta'N$  interaction. In view of the relatively low production rate, until recently there existed only a very limited number of experimental studies of  $\eta'$  production reactions. However, the situation has changed in the past few years, especially in  $\eta'$  photoproduction, where high-precision data for both nucleon and deuteron targets have become available [6–8]. Also, the  $pp$  and  $pn\eta'$  invariant-mass distribution data in the  $pp \rightarrow pp\eta'$  reaction are now available [9], in addition to the cross section data [10–12]. Upper limits for the total cross sections in  $pn \rightarrow pn\eta'$  have also been reported [13]. Consideration of the high-precision cross section data in free  $\gamma p \rightarrow \eta'p$  [6] that have only become available recently, together with the cross section data on quasi-free  $\gamma n \rightarrow \eta'n$  [8] and the invariant mass distribution data in  $pp \rightarrow pp\eta'$  [9], impose sufficient constraints to unambiguously determine the set of minimal spin-1/2 and -3/2 resonances necessary, in principle, for an adequate reproduction of the data [14].

The  $\eta'$  meson production reactions mentioned above are described based on an effective Lagrangian approach. For the two-body photon- and pion-induced reactions, it is shown that the present results are consistent with very small final state (transition) interactions. For  $NN \rightarrow NN\eta'$ , both the initial and final state  $NN$  interactions are taken into account explicitly in the Distorted Wave Born Approximation. The photoproduction reaction

amplitude in our model is gauge invariant and, as such, it obeys the generalized Ward–Takahashi identity. The dynamical content of the present model can be found in Ref. [14].

## 2. Results

As mentioned in the previous section, a combined analysis of the  $\gamma N \rightarrow \eta' N$ ,  $\pi N \rightarrow \eta' N$  and  $NN \rightarrow NN\eta'$  reactions is performed in the present work. Considering spin-1/2 and -3/2 resonances, we found that a set of above-threshold resonances  $\{S_{11}, P_{11}, P_{13}\}$ , with fitted mass values of about  $M_R = 1925, 2130$ , and  $2050$  MeV, respectively, and the four-star sub-threshold  $P_{13}(1720)$  resonance reproduce best all existing data for the  $\eta'$  production processes from threshold to  $\sqrt{s} \sim 2.35$  GeV. All three above-threshold resonances found in the present analysis are essential and indispensable for the good quality of the present fits.

In the free  $\gamma p \rightarrow \eta' p$  reaction, there is discrepancy between the CLAS [6] and CBELSA/TAPS [7] data. Thus, we consider them separately in our combined analysis of  $\eta'$  production processes. Figure 1 shows our resulting independent fit curves for the respective data. We see that both data sets are reproduced very well. All the resonance masses and widths from the fit to CLAS data are very close to those from the fit to CBELSA/TAPS data, except for the width of  $P_{13}(2050)$  resonance, for which the CBELSA/TAPS data yield a much narrower width, however, with a very large uncertainty.

Figure 2 shows the individual resonance contributions to the predicted total cross sections obtained by integrating the differential cross section results shown in Fig. 1 for the CLAS (left panel) and CBELSA/TAPS (right panel) data. For resonance contributions, we see significant differences in their relative contributions. The  $P_{11}$  resonance contribution is much stronger for CBELSA/TAPS than for CLAS, which is responsible for making the full total cross section larger for energies above  $W \sim 2.1$  GeV. For both data sets, the respective  $S_{11}$  resonance contributions alone are responsible for the sharp rise of the full total cross section (gray/red curves) near threshold, and their corresponding parameter sets are practically identical. The clear peak structure in the full total cross section exhibited by the CBELSA/TAPS data is produced here by the above-threshold  $P_{13}$  resonance which is much narrower for the CBELSA/TAPS data than for CLAS. However, the uncertainty associated with its width is very large and this width, therefore, is not well constrained. The origin of this large uncertainty in the width can be traced back to the CBELSA/TAPS measured differential cross sections at one particular energy only, namely at  $W = 2.052$  GeV, which coincides with the  $P_{13}$  resonance whose position is fixed very well within our fits with very small errors for both data sets. In view of the large error for the  $P_{13}$  width for the CBELSA/TAPS data, there is no physical significance in find-

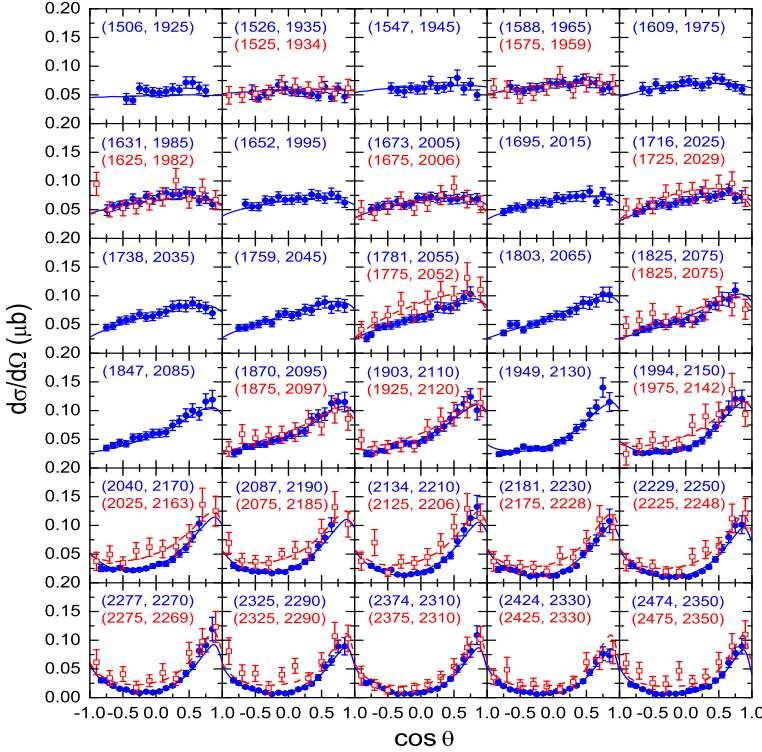


Fig. 1. (Color online) Differential cross sections for free  $\gamma p \rightarrow \eta' p$ . The black/blue and gray/red curves are our results fitted to CLAS data [6] (filled circles) and CBELSA/TAPS data [7] (empty squares), respectively.

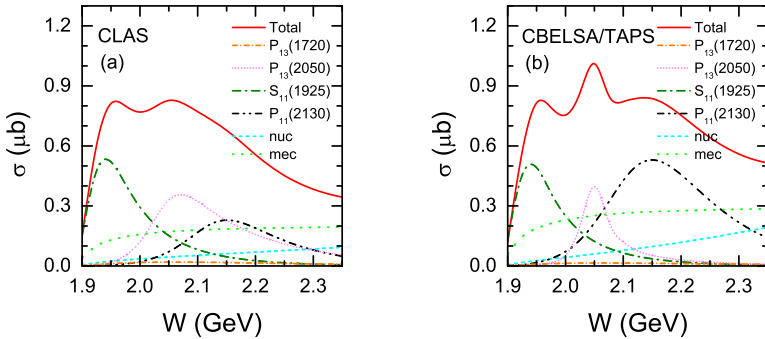


Fig. 2. (Color online) Total cross sections with individual (nucleonic, mesonic, and resonance) current contributions. The left panel (a) results from the fit to the CLAS data, while the right panel (b) pertains to the CBELSA/TAPS data. The peak structure at 2.05 GeV for the latter data is solely due to the narrow  $P_{13}(2050)$  resonance.

ing the peak structure shown in Fig. 2. The main conclusion regarding the discrepancy between the CLAS [6] and CBELSA/TAPS [7] data as exhibited in Fig. 1 is that the larger cross section yield of the CBELSA/TAPS data at higher energies results in a larger  $P_{11}$  resonance contribution compared to the CLAS data. This alone largely leads to the enhancement of the CBELSA/TAPS total cross section over the CLAS results seen in Fig. 2 for energies above  $W \sim 2.1$  GeV. For future analyses, it is important to resolve this discrepancy in the findings of the CLAS and CBELSA/TAPS experiments if one is to obtain more definitive answers about these above-threshold resonances.

Figure 3 shows our results for quasi-free  $\gamma n \rightarrow \eta' n$ . We see that overall, the data are reproduced reasonably well. To describe the quasi-free process, we have folded the corresponding free-process cross sections with the momentum distribution of the neutron inside the deuteron.

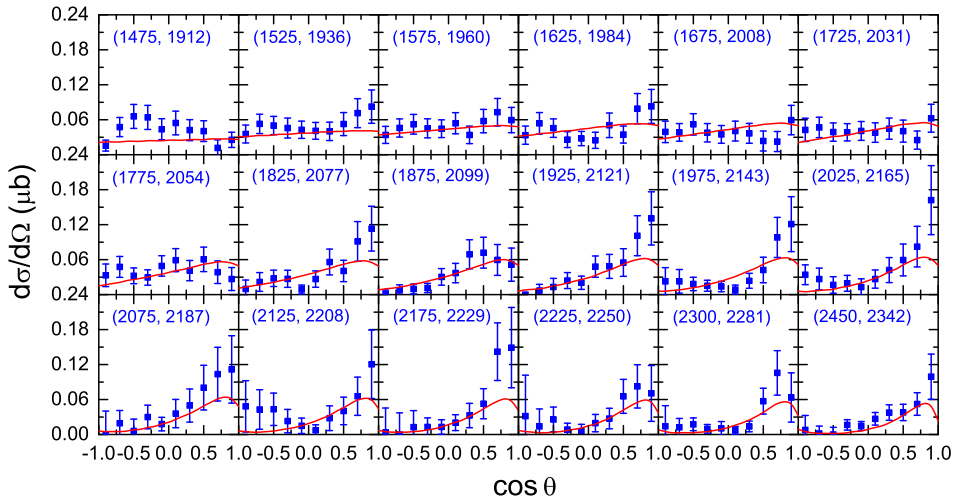


Fig. 3. (Color online) Differential cross sections for quasi-free  $\gamma n \rightarrow \eta' n$ . The solid curves are our results fitted to the CBELSA/TAPS quasi-free data [8] (solid squares).

Our result for the  $pp \rightarrow pp\eta'$  total cross section is shown in Fig. 4. We see that the data are nicely reproduced over a wide range of excess energy. The dynamical content of the present model is also displayed. One sees that the spin-1/2 and -3/2 resonance contributions have different energy dependences. In the lower excess-energy region, the spin-1/2 resonance contribution is only slightly smaller than the spin-3/2 resonance contribution, but as the energy increases, the spin-3/2 resonance contribution starts to dominate. Here, the dominant spin-3/2 resonance contribution is due to the  $P_{13}(2050)$ ,

while the dominant spin-1/2 resonance contribution is from the  $S_{11}(1925)$  resonance. The result for the  $pn \rightarrow pn\eta'$  total cross section is also shown in Fig. 4. The  $pn\eta'$  together with the  $pp\eta'$  reactions helps constraining the isoscalar– and isovector–meson couplings to the resonances. Unfortunately, only the upper limit of the cross section in a limited energy range is currently available for the  $pn\eta'$  process. Therefore, the isoscalar–isovector meson exchange content of the present model is subject to this limitation in the existing data.

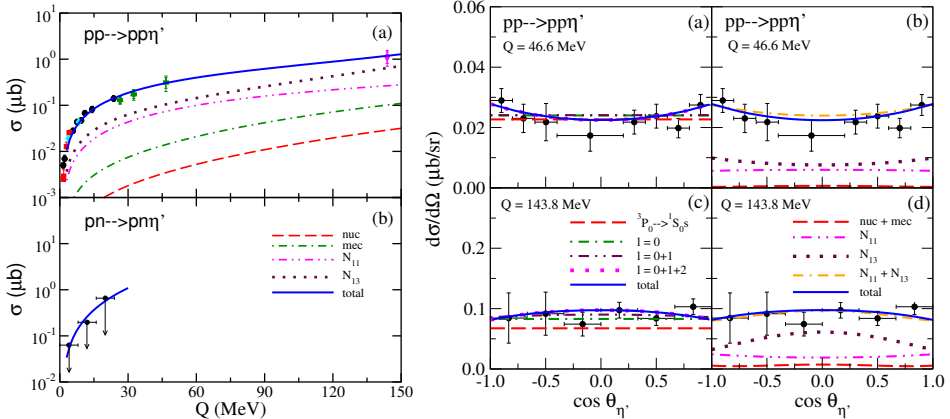


Fig. 4. (Color online) Right panel: total cross sections (black/blue solid curves) for  $pp \rightarrow pp\eta'$  (right panel (a)) and  $pn \rightarrow pn\eta'$  (right panel (b)) as functions of excess energy  $Q$ . For  $pp\eta'$ , the individual current contributions are: nucleonic current (long-dashed/red curve), mesonic current (dash-dotted/green),  $N_{11} = S_{11}(1925) + P_{11}(2130)$  resonance current (dash-double-dotted/magenta),  $N_{13} = P_{13}(1720) + P_{13}(2050)$  (dotted/maroon). The  $pp\eta'$  data are from Refs. [10–12]; the  $pn\eta'$  data, which are upper limits, are from Ref. [13]. Left panel:  $\eta'$  angular distribution in  $pp \rightarrow pp\eta'$  in the center-of-momentum frame of the system for two excess energies of  $Q = 46.6$  and  $143.8$  MeV. The solid curves show our results from full calculation. The panels in left-hand side column show the contributions from the partial waves, and the panels in the right-hand side column show the contributions from individual currents.

Figure 4 also shows our results for the  $\eta'$  angular distribution in  $pp \rightarrow pp\eta'$  at the excess energies of  $Q = 46.6$  and  $143.8$  MeV, and Fig. 5 shows the  $\pi N \rightarrow \eta' N$  total cross sections. These results are obtained in conjunction with the CLAS photoproduction data. Again, all the data are reproduced quite well. We emphasize that in a combined analysis of  $\eta'$  photon- and hadron-induced reactions,  $\{P_{13}(1720), S_{11}(1925), P_{13}(2050), P_{11}(2130)\}$  is the minimum set of resonances to describe well all the existing ones.

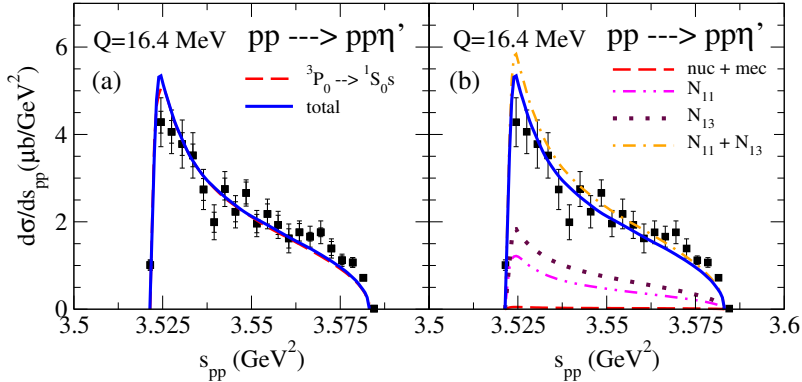


Fig. 5. (Color online) The  $pp$  invariant mass distributions in  $pp \rightarrow pp\eta'$  at an excess energy of  $Q = 16.4$  MeV. The black/blue solid curves correspond to the full result. The left panel (a) shows the  $^3P_0 \rightarrow ^1S_0s$  (dashed/red curve) partial wave contributions. The right panel (b) shows the nucleonic+mesonic currents (dashed/red), the spin-1/2 resonances (dash-dotted/green), the spin-3/2 resonances (dash-double-dotted/magenta), and the sum of the spin-1/2 and -3/2 resonances (dotted/maroon) contributions. The data are from Ref. [9].

Figure 5 shows our results for the  $pp$  invariant mass distribution in  $pp \rightarrow pp\eta'$  revealing a good agreement with the COSY-11 data [9]. In the left panel of Fig. 5, one sees that the  $pp$  invariant mass distribution is practically exhausted by the  $^3P_0 \rightarrow ^1S_0s$  partial wave. This is quite surprising in view of the findings of Ref. [15] mentioned above, where a significant final-state  $P$ -wave contribution was found in the higher  $pp$  invariant mass region in the  $pp \rightarrow pp\eta$  reaction. The present finding implies that the  $S$ -wave basic production amplitude in the present model should have an energy dependence as proposed in Ref. [16], since the  $pp$  invariant-mass dependence introduced by the  $pp$  final-state interaction (FSI) is not enough to account for the enhancement of the measured  $pp$  invariant-mass distribution at larger invariant masses. This finding tells us that the conclusion reached in Ref. [9] ruling out the  $\eta N$  FSI as a possible source of the enhancement in the  $pp$  invariant mass distribution at larger invariant mass values based on the comparison of the corresponding shapes in  $pp\eta$  and  $pp\eta'$  has to be taken with caution, since there might be different mechanisms operating in these reactions as shown explicitly here in Fig. 5. At this stage, it is natural to ask what the underlying dynamics is in the  $S$ -wave contribution that accounts for the enhancement of the  $pp$  invariant mass distribution at larger invariant mass values in  $pp \rightarrow pp\eta'$  as compared to that in the  $pp \rightarrow pp\eta$  reaction, where the enhancement arises from the  $^1S_0 \rightarrow ^3P_0s$  partial wave. In the right panel of Fig. 5, we show the individual current contribution

to the  $pp$  invariant-mass distribution. We see that the enhancement at higher values of invariant mass is largely due to the constructive interference between the spin-1/2 and the spin-3/2 resonance contributions.

The left panel of Fig. 6 shows the  $\pi N \rightarrow \eta' N$  total cross sections. Unfortunately, as one can see, this reaction offers only an order-of-magnitude constraint of the model due to the large uncertainty in the data. An interesting feature of the present model results is the double-bump structure caused by the  $S_{11}(1925)$  and an interplay of the  $P_{13}(2050)$  and  $P_{11}(2130)$  resonances. The  $S_{11}(1925)$  resonance is just about 20 MeV above threshold. In view of their large uncertainties, the currently existing data shown in Fig. 6 can indeed accommodate such a structure; however, clearly more accurate data are needed for a definitive answer. If experimentally corroborated, such a bump structure would rule out the subthreshold resonance-dominance assumption of Ref. [29], where  $S_{11}(1535)$  resonance dominance is assumed to describe both the  $\pi N \rightarrow \eta' N$  and  $NN \rightarrow NN\eta'$  cross section data, since it is not possible to generate any bump structure from sub-threshold resonances alone. The right panel of Fig. 6 reveals that the dominant contribution is by far the  $s$ -channel contribution. This result shows that the  $\eta' N$  FSI, which is associated with the non-pole part of the  $T$ -matrix, is consistent with being very small. In particular, here, one gets the  $\eta' N$  scattering length of  $a_{\eta' N} \sim 0.017 + i0.005$  fm.

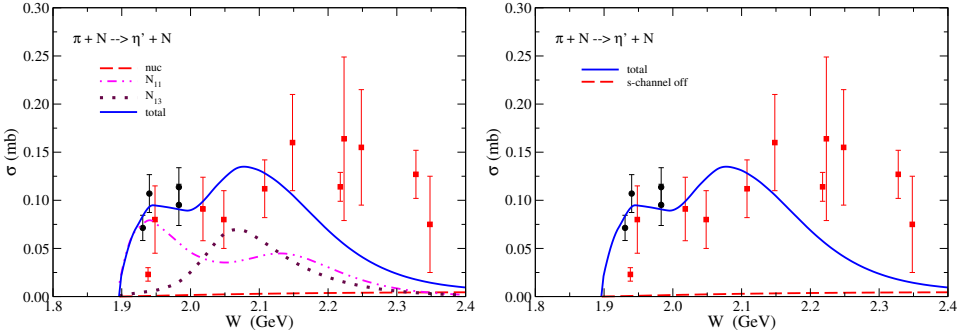


Fig. 6. (Color online) Total cross section for  $\pi N \rightarrow \eta' N$  as a function of the total energy of the system. The black/blue solid curves corresponds to the full results, determined in conjunction with the fit to the  $\gamma N \rightarrow \eta' N$  as well as the  $NN \rightarrow NN\eta'$  data. The individual current contributions are also show: nucleonic current (dashed/red curve),  $N_{11} = S_{11}(1925) + P_{11}(2130)$  resonance current (dash-double-dotted/magenta ), and  $N_{13} = P_{13}(1720) + P_{13}(2050)$  (dotted/maroon). Data for  $\pi^- p \rightarrow \eta' n$  (black solid circle) and for  $\pi^+ n \rightarrow \eta' p$  (gray/red solid square) are from Refs. [17–19].

### 3. Summary

Based on an effective Lagrangian approach, we have performed a combined analysis of the free and quasi-free  $\gamma N \rightarrow \eta' N$ ,  $NN \rightarrow NN\eta'$ , and  $\pi N \rightarrow \eta' N$  reactions. Considering spin-1/2 and -3/2 resonances, we have found that a set of above-threshold resonances  $\{S_{11}, P_{11}, P_{13}\}$ , with fitted mass values of about  $M_R = 1925, 2130$ , and  $2050$  MeV, respectively, and the four-star sub-threshold  $P_{13}(1720)$  resonance reproduce best all existing data for the  $\eta'$  production processes from threshold to  $\sqrt{s} \sim 2.35$  GeV. All three above-threshold resonances found in the present analysis are essential and indispensable for the good quality of the present fits. Of course, higher spin resonances may (and probably will) contribute to the  $\eta'$  production processes. However, their consideration within the present model leads to an overdetermination of the currently available data, and therefore they cannot be determined unambiguously. In this regard, other independent observables, especially the spin observables, are badly needed. In fact, beam and beam-target symmetries are current being measured by the CLAS [20] and CBESLA/TAPS [21] Collaborations, respectively.

The present model yields a very small  $\eta' N$  scattering length of  $a_{\eta' N} \sim 0.017 + i0.005$  fm. Whether such a small scattering length can lead to a formation of  $\eta'$ -mesic nuclei remains to be seen. For one, what determines the existence of such a bound state is the strength of the interaction in the nuclear medium and not in free space (see, *e.g.*, Ref. [22]). Also, our value of the scattering length may change once a full coupled channels calculation with all the members of the SU(3) nonet of mesons are taken into account [23].

The material presented here resulted from a collaboration with Fei Huang, Helmut Haberzettl and Shahab Rezav Hessabi. This work was supported by the FFE-COSY Grant No. 41788390 (COSY-58).

### REFERENCES

- [1] S. Capstick, N. Isgur, *Phys. Rev.* **D34**, 2809 (1986); S. Capstick, W. Roberts, *Phys. Rev.* **D47**, 1994 (1993); **D49**, 4570 (1994); **D57**, 4301 (1998); **D58**, 074011 (1998).
- [2] K. Itahashi, *Acta Phys. Pol. B* **45**, 731 (2014), this issue; talk by M. Nanova at the II International Symposium on Mesic Nuclei, Kraków, Poland, September 22–25, 2013.
- [3] R.A. Arndt *et al.*, *Phys. Rev.* **C72**, 045202 (2005).
- [4] E. Oset, A. Ramos, *Phys. Lett.* **B704**, 334 (2011).
- [5] P. Moskal *et al.*, *Phys. Lett.* **B482**, 356 (2000).

- [6] M. Williams *et al.*, *Phys. Rev.* **C80**, 045213 (2009).
- [7] V. Crede *et al.*, *Phys. Rev.* **C80**, 055202 (2009).
- [8] I. Jaegle *et al.*, *Eur. Phys. J.* **A47**, 11 (2011).
- [9] P. Klaja *et al.*, *Phys. Lett.* **B684**, 11 (2010).
- [10] F. Hibou *et al.*, *Phys. Lett.* **B438**, 41 (1998); P. Moskal *et al.*, *Phys. Rev. Lett.* **80**, 3202 (1998); P. Moskal *et al.*, *Phys. Lett.* **B474**, 416 (2000).
- [11] F. Balestra *et al.*, *Phys. Lett.* **B491**, 29 (2000).
- [12] A. Khoukaz *et al.* [COSY-11 Collaboration], *Eur. Phys. J.* **A20**, 345 (2004).
- [13] J. Klaja *et al.*, *Phys. Rev.* **C81**, 035209 (2010).
- [14] F. Huang, H. Haberzettl, K. Nakayama, *Phys. Rev.* **C87**, 054004 (2013).
- [15] K. Nakayama, J. Haidenbauer, C. Hanhart, J. Speth, *Phys. Rev.* **C68**, 045201 (2003).
- [16] A. Deloff, *Phys. Rev.* **C69**, 035206 (2004).
- [17] J.P. Dufey *et al.*, *Phys. Lett.* **B26**, 410 (1968); M. Basile *et al.*, *Nuovo Cim.* **A3**, 371 (1971); M. Basile *et al.*, *Nucl. Phys.* **B33**, 29 (1971).
- [18] P.K. Rader *et al.*, *Phys. Rev.* **D6**, 3059 (1972); J. Bensinger, A.R. Erwin, M.A. Thompson, W.D. Walker, *Phys. Lett.* **B33**, 505 (1970); R.J. Miller, S. Lichtman, R.B. Willmann, *Phys. Rev.* **178**, 2061 (1969).
- [19] A. Baldini, V. Flaminio, W.G. Moorhead, D.R.O. Morrison, *Total Cross-Sections for Reactions of High Energy Particles*, Landolt-Börnstein, edited by H. Schopper, Springer, Berlin, 1988, Vol I/12a.
- [20] P. Collins *et al.*, to be published.
- [21] F.N. Afzal [CBELSA/TAPS Collaboration], *EPJ Web of Conferences* **37**, 09001 (2012).
- [22] S. Sakai, D. Jido, *Phys. Rev.* **C88**, 064906 (2013) [[arXiv:1309.4845 \[nucl-th\]](https://arxiv.org/abs/1309.4845)].
- [23] D. Rönchen *et al.*, *Eur. Phys. J.* **A49**, 44 (2013).